Large Neutral Barrier at Grain Boundaries in Chalcopyrite Thin Films

Michael Hafemeister,[1] Susanne Siebentritt,[2] Jürgen Albert,[1] Martha Ch. Lux-Steiner,[1] and Sascha Sadewasser[1,*]

[1]*Helmholtz-Zentrum Berlin für Materialien und Energie, Hahn-Meitner-Platz 1, 14109 Berlin, Germany*

[2]*Université du Luxembourg, Laboratoire de photovoltaique, 41, rue du Brill, L-4422 Belvaux*

(Received 6 January 2010; published 14 May 2010)

The electronic structure of grain boundaries in polycrystalline Cu(In, Ga)Se_2 thin films and their role on solar cell device efficiency is currently under intense investigation. A neutral barrier of about 0.5 eV has been suggested as the reason for the benign behavior of grain boundaries in chalcopyrites. Previous experimental investigations have in fact shown a neutral barrier but only a few 10 meV high, which cannot be expected to have a significant influence on the solar cell efficiency. Here we show that a full investigation of the electrical behavior of charged and neutral grain boundaries shows the existence of an additional narrow neutral barrier, several 100 meV high, which is tunneled through by the majority carriers but is sufficiently high to explain the benign behavior of the grain boundaries.

DOI: 10.1103/PhysRevLett.104.196602 PACS numbers: 72.80.Ey, 61.72.Mm, 71.55.Gs, 72.20.−i

Understanding the impact of grain boundaries (GBs) on electronic material properties has been a challenge in a variety of polycrystalline materials, as superconductors [1,2], perovskites [3], polymers [4], and semiconductors [5,6]. Despite the abundance of GBs in polycrystalline chalcopyrite—Cu(In, Ga)Se_2 (CIGSe)—thin films, solar cells based on this materials system reach surprisingly high power conversion efficiencies of up to 20% [7]. In contrast, for single crystalline Si and III-V solar cell materials GBs are known to have a strong detrimental effect on device efficiencies due to defects located at the GBs and the related recombination losses.

Currently, different models are proposed to describe the GB properties in *p*-type CIGSe [8]. In the classical GB model it was proposed that charged defects are located in the GB plane from which a space charge region (SCR) develops into the grain [9,10]. The resulting band bending presents a barrier for majority carrier transport. This model is used to describe GBs in polycrystalline Si and cannot account for the reduced recombination at GBs in chalcopyrites. To explain this benign behavior two models have been presented. For twin boundaries ($\Sigma 3$-GBs [11]) a Cu depletion in the $\{112\}_{\text{tet}}$ GB plane [12] is assumed [13,14], similar to the one proposed for $\{112\}_{\text{tet}}$-oriented polar surfaces [15,16], which are stabilized by the formation of Cu vacancies V_{Cu}^{-}. The reduced Cu content results in a lowering of the valence band edge [13], thereby forming a barrier for majority carrier transport of about 0.5 eV. However, another density function theory (DFT) study on a $\Sigma 3$-GB did not assume Cu depletion and did not confirm the lowering of the valence band edge [17]. A different model to explain the benign behavior of CIGSe GBs was presented for a differently oriented GB along the $\{11\bar{4}\}_{\text{tet}}$ plane in CISe; DFT calculations by Yan *et al.* [18] provide evidence for a lattice relaxation around the GB, where dangling bond defect levels shift from the band gap into the valence band, thereby reducing GB recombination. The theoretically predicted neutral transport barrier due to a valence band offset at the $\Sigma 3$ twin GB [13,14] could be confirmed experimentally using a combination of Hall mobility and Kelvin probe force microscopy (KPFM) measurements [19]. In the latter study a macroscopic bicrystal allowed the majority carrier transport measurement across an individual GB, confirming the presence of a charge neutral barrier, however of only ~30 meV.

The effect of the different GB models on the device efficiency was analyzed by means of two-dimensional (2D) device simulations with two main results: (i) the SCR around a charged GB leads to an enhanced electron collection at the cost of a loss in open circuit voltage [20]; (ii) in order to effectively reduce GB recombination by means of a valence band offset, this has to be at least 300 meV [21]. The simulations assume GB widths between 2 and 20 nm; however, transport across the GBs via a tunneling process was not included.

In this Letter we present a study on a single charged $\Sigma 9$ GB and a single neutral $\Sigma 3$ GB in *p*-type $CuGaSe_2$ obtained by epitaxial growth on GaAs bicrystals. The charge state of the GBs is obtained from KPFM measurements. In contrast to the previous interpretation of the electrical transport measurements, where only the mobility was taken into account, we model now the resistance of the GB and find that it is dominated by tunneling through a barrier of several 100 meV.

To obtain macroscopic $CuGaSe_2$ bicrystals where the two grains are separated by a single GB, we grew $CuGaSe_2$ on top of GaAs bicrystals by metal organic vapor phase epitaxy [19]. One GaAs wafer [22] consists of two grains exhibiting a $\{536\}_{\text{cub}}$ and $\{525\}_{\text{cub}}$ surface [12]. The grains can be transformed into each other by a rotation of 90° along the $\langle 212\rangle_{\text{cub}}$ direction, as confirmed by electron backscatter diffraction (EBSD) (not shown) [22]; thus, the grains are separated by a $\Sigma 9$ GB [11]. On both grains successful epitaxial growth was achieved, as confirmed by EBSD. The GB in the $CuGaSe_2$ film presents a direct continuation of the GB in the GaAs substrate and the GB

plane shows a $\{111\}_{tet}$ orientation. The preparation of the $\Sigma 3$-GB was previously described [19]. The electronic properties of the GBs were investigated by KPFM and temperature dependent Hall-effect and resistivity measurements.

KPFM measures the electrostatic interaction between an atomic force microscope (AFM) tip and the sample and serves to determine locally accumulated charge. The ultrahigh vacuum ($p < 10^{-10}$ mbar) KPFM (Omicron) determines the sample topography in frequency modulation AFM [23] using an oscillation amplitude of ≈ 20 nm at the fundamental resonance frequency ($f_0 \approx 75$ kHz) of the PtIr-coated cantilever (Nanosensors). The contact potential difference (CPD) was measured using the second oscillation mode of the cantilever ($f_2 \approx 470$ kHz) applying an ac bias of $V_{ac} = 100$ mV [19,24].

For Hall measurements the samples are divided into three pieces. On two pieces on each side of the GB the bulk values of resistivity, charge carrier concentration and mobility are measured by the van der Pauw method. One piece containing the GB is provided with stripe contacts (distance = 0.8 mm) for conductivity measurements across the GB using the four point method. The resistance and Hall mobility were analyzed according to previously published procedures [19].

A KPFM measurement of the two grains including the $\Sigma 9$-GB is shown in Fig. 1. Because of a slightly different growth rate of the $CuGaSe_2$ on the differently oriented surfaces of the GaAs bicrystal substrate a step of ~ 100 nm develops at the GB. Along the GB a dip in the CPD is observed, which amounts to ~ 90 mV. The two sides of the dip show the characteristic shape of a SCR extending ≈ 280 nm into the grain. Therefore, we conclude that the $\Sigma 9$-GB exhibits the presence of charged defects, in clear contrast to the previously studied neutral $\Sigma 3$-GB [19]; this is in qualitative agreement with the expected higher defect concentration at the higher disorder $\Sigma 9$-GB. The SCR shields fixed charges at the GB and can be described by

$$\phi_{SCR}(x) = \phi_{ch}\left(1 - \frac{|x|}{w}\right)^2, \tag{1}$$

where ϕ_{ch} is the potential energy of the charged barrier and w the SCR width given by $w^2 = \frac{2\epsilon_r \epsilon_0 \phi_{ch}}{e^2 p}$. Here, $\epsilon_r = 11$ [25] and ϵ_0 are the dielectric constant of the semiconductor and the vacuum, respectively, and e and p are the elemental charge and the charge carrier concentration of the semiconductor, respectively.

The big advantage of a large bicrystal compared to a polycrystalline sample is the possibility to perform electrical measurements on one specific GB as opposed to averaging over many GBs. The temperature dependent mobility of majority carriers [19] across the $\Sigma 9$-GB is shown in Fig. 2(a) and can be well described by the Arrhenius dependence (solid line) for thermally activated transport across a barrier of $\phi_{mob} = (100 \pm 10)$ meV. This value is considerably larger than the one found previously for $\Sigma 3$-GBs [19], but it is in good agreement with the barrier found in the KPFM measurements (Fig. 1).

In view of this we simulate the transport across the $\Sigma 9$-GB assuming a thermionic emission (TE) mechanism. Tunneling is not considered for this barrier due to the large width. Seto [9] described the thermionic emission current J_{TE} for small applied voltage V:

$$J_{TE} = e^2 p V \left(\frac{1}{2\pi m^* k_B T}\right)^{1/2} \exp\left(-\frac{\Delta\phi}{k_B T}\right), \tag{2}$$

where k_B is the Boltzmann constant, p the hole concentration, $m^* = 1.2 m_e$ the effective mass of the carriers [26], and the considered barrier is $\Delta\phi = \phi_{mob} \approx \phi_{ch}$.

Considering the measured temperature dependence of the hole concentration $p(T)$ (not shown) the temperature dependent resistance across the $\Sigma 9$-GB is simulated and shown (open triangles) together with the actually measured resistance (solid squares) in Fig. 2(b). It is obvious, that the transport by TE using the transport barrier determined from KPFM and Hall mobility is insufficient to explain the experimental temperature dependent resistance; in fact

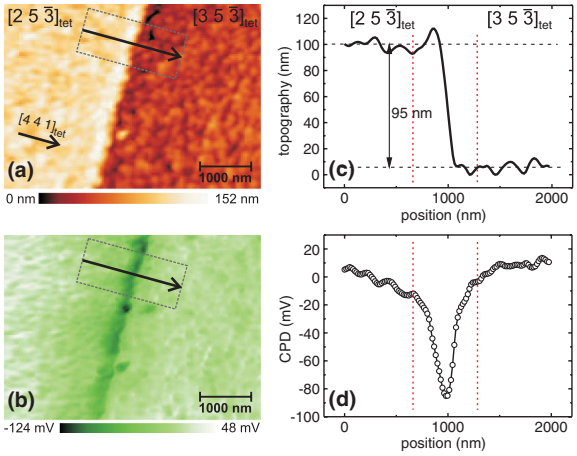

FIG. 1 (color online). KPFM measurement on the $CuGaSe_2$ bicrystal containing a $\Sigma 9$ grain boundary. (a) Topography and (b) CPD showing a dip along the GB. Averaged line profiles across the GB were extracted in the gray box indicated in the images for (c) topography and (d) CPD.

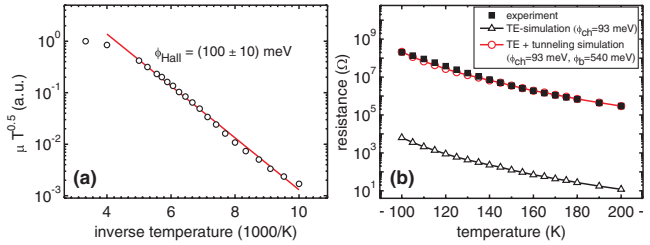

FIG. 2 (color online). (a) Hall mobility of the $\Sigma 9$-GB showing a thermally activated barrier of ~ 100 meV. (b) Temperature dependence of the resistance for transport across the $\Sigma 9$-GB (solid squares) with fits considering only TE (open triangles) and TE and tunneling (open circles).

the discrepancy amounts to more than 4 orders of magnitude. We therefore introduce an additional thin barrier, similar to what has been proposed previously for GB transport in Si [27] and GaAs [28]; typically, the thin barrier is assigned to a scattering potential with a width of a few lattice planes. We assume here the width b_b of our thin barrier to be equal to the distance of 6 lattice planes (3 in each direction of the GB) in the $\langle 441\rangle_{\mathrm{tet}}$ direction perpendicular to the $\{111\}_{\mathrm{tet}}$ GB plane, namely $b_b = 1.36$ nm [29]. The height of this additional barrier will be extracted from a fit to the experimental resistance. The resulting electronic structure of the GB is displayed in Fig. 3. The transport across this GB barrier will be described by a TE current and a contribution from tunneling (T) through the barrier [27]:

$$J_{\mathrm{total}} = J_{\mathrm{TE}} + J_T = e^2 p \beta V \left(\frac{\beta}{2\pi m^*}\right)^{1/2} \left[\int_0^{\phi_{\mathrm{ch}}} e^{-\beta E} \tau_{\mathrm{SCR}}(E)\tau_b(E)dE + \int_{\phi_{\mathrm{ch}}}^{\phi_b} e^{-\beta E}\tau_b(E)dE + \int_{\phi_b}^{\infty} e^{-\beta E}dE\right], \quad (3)$$

where $\beta = (k_B T)^{-1}$. The first integral describes the tunneling contribution through the SCR and the thin barrier where the transmission probability is given by the approximation for a wide barrier:

$$\tau_{\mathrm{SCR}}(E) = \exp\left(-\frac{4\pi}{h}\int_{-a}^{a}\sqrt{2m^*(\phi_{\mathrm{SCR}}(x) - E)}dx\right), \quad (5)$$

where $\phi_{\mathrm{SCR}}(x)$ is given by Eq. (1) and a is the classical turning point of carriers with energy E. The second integral in Eq. (3) describes the tunneling through the thin barrier where the transmission probability is given by

$$\tau_b(E) = \left[1 + \frac{\phi_b^2}{4E(\phi_b - E)}\sinh^2(\kappa b_b)\right]^{-1}, \quad (6)$$

with $\kappa = [8\pi^2 m^*(\phi_b - E)/h^2]^{1/2}$ [30]. The third integral in Eq. (3) describes the TE across the whole barrier, for energies higher than the thin barrier ϕ_b.

Using the barrier schematically presented in Fig. 3 and Eq. (3), the temperature dependence of the resistance of the GB is simulated and the barrier height ϕ_b is extracted. As shown in Fig. 2(b), the simulated resistance (open circles) gives an excellent fit to the experimental data (solid squares), using a charged barrier of $\phi_{\mathrm{ch}} = (93 \pm 10)$ meV and a thin barrier of $\phi_b = (540 \pm 50)$ meV. The charged barrier height ϕ_{ch} is in excellent agreement with the values determined by Hall mobility and KPFM.

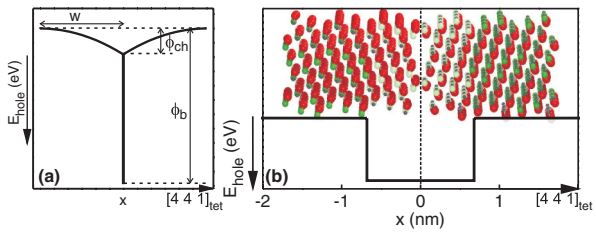

FIG. 3 (color online). (a) Electronic structure model of the Σ9-GB, consisting of a rectangular barrier and a SCR, used for simulating the electrical transport by Eq. (3). (b) Detailed view of the region close to the GB plane, including an atomistic sphere model (Cu—medium green, Ga—small gray, Se—large red).

In our previous characterization of a Σ3-GB [19] we found a charge neutral transport barrier of ~30 meV. In view of the above presented analysis, we now reconsider the electronic structure of this Σ3-GB and investigate also its temperature dependent resistance. Figure 4(a) shows that the simulated resistance considering only TE over a 30 meV barrier (open triangles) is considerably lower (2–3 orders of magnitude) than the experimentally determined resistance (solid squares). Therefore, we also include an additional thin barrier at this Σ3-GB surrounded by the previously determined small rectangular barrier, leading to the proposed electronic structure shown in Fig. 4(b). In this case, we do not assume the presence of a SCR, as KPFM experiments did not show any evidence of charges at the Σ3-GB [19]. We set the width of the high barrier to 6 lattice planes in the $\langle 221\rangle_{\mathrm{tet}}$ direction perpendicular to the GB plane, which corresponds to 1.93 nm [29]. The height ϕ_b of this barrier will be extracted from the fit to the experimental data. The surrounding barrier width is assumed to be 3 lattice planes on each side (=0.96 nm) and its height is fixed to the barrier determined from the mobility measurements, $\phi_0 = 30$ meV [19]. Considering the combined transport by TE and tunneling according to Eq. (3), the experimental data can be well fitted (open circles) using $\phi_b = (170 \pm 25)$ meV [Fig. 4(a)].

It is apparent from the analysis of the temperature dependent GB resistance of the Σ3- and Σ9-GBs that the transport across the GB requires the inclusion of a thin and high rectangular barrier. Up to now, the presence of such a potential has not been considered for the electronic structure of chalcopyrite GBs. For GBs in other semiconductor materials such a thin barrier is ascribed to a scattering potential [27,28]; the origin is not clearly understood and is usually ascribed to the presence of defects and/or impurity atoms. We now discuss the possible origin of the rectangular barrier at chalcopyrite GBs. In the present samples consisting in high purity bicrystal samples grown on GaAs wafers, a large effect due to impurity atoms should be minimal in comparison to polycrystalline material grown on glass substrates. However, chalcopyrites contain a large amount of intrinsic defects, which could be present at the GBs. Thus, also in the present case the origin of the scattering potential could be assigned to defects. In the case of the Σ3-GB, the GB plane corresponds to the $\{112\}_{\mathrm{tet}}$ plane, which has been proposed to be Cu depleted [13,14]. The formation of Cu vacancies [15,16] results in a steplike valence band offset at the GB plane, which possibly corresponds to the observed barrier for majority carrier transport. The theoretically proposed magnitude of the valence band offset for

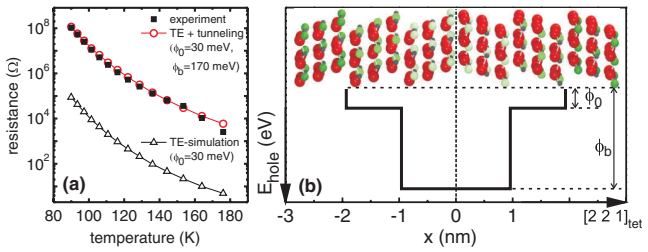

FIG. 4 (color online). (a) Temperature dependence of the resistance of the Σ3-GB (solid squares) and fits using only TE (open triangles) and a combination of TE and tunneling (open circles), considering the (b) electronic structure model comprising a high and thin barrier (ϕ_b) surrounded by lower rectangular barriers (ϕ_0) and an atomistic sphere model (same colors as in Fig. 3).

$CuGaSe_2$ is ~0.5 eV [13] and agrees fairly well with the barrier height obtained from our experimental fits (0.2–0.6 eV). These values are also in agreement with a widened band gap at Cu-poor CIGSe surfaces observed by Heske *et al.* [31,32]. Also for other GB orientations the formation of Cu vacancies (indicated by the weaker colors in the atomistic models in Figs. 3 and 4) has been shown to be favorable [18].

We would like to point out, that the observed dip in the KPFM measurements of the Σ9-GB is in excellent agreement to results reported for polycrystalline CIGSe films [33–35]. However, it has to be considered that polycrystalline films show the presence of a variety of different GB types [36]. 2D device simulations considering the effects of GBs have predicted a negligible influence of GB recombination only in the case of a GB barrier larger than ~0.3 eV [21]. The above concluded barriers at the Σ3- and Σ9-GBs are in good agreement with this requirement. However, the effect of tunneling was not included in these simulations. Nevertheless, a possible recombination of holes at GB defects should be reduced, as the probability density of the carriers is considerably reduced in the barrier. Therefore, the presented results and analysis present a major improvement of the understanding of the physics of chalcopyrite GBs and their role in device operation.

In conclusion, we have shown that a sufficiently high neutral barrier exists at charged and neutral GBs and at GBs for which Cu depletion is predicted [13] and at such, where it is not predicted [18]. The barrier height is sufficient to reduce GB recombination; however the models predicting the necessary barrier height did not include tunneling. Our results point out the importance of tunneling transport through GB barriers, as well in chalcopyrite materials, as in other semiconductors.

The authors acknowledge funding by the Deutsche Forschungsgemeinschaft (DFG) and helpful discussions with S. Lehmann.

*sadewasser@helmholtz-berlin.de

[1] D. Dimos, P. Chaudhari, J. Mannhart, and F. K. LeGoues, Phys. Rev. Lett. **61**, 219 (1988).
[2] G. Hammerl *et al.*, Nature (London) **407**, 162 (2000).
[3] M. Kim *et al.*, Phys. Rev. Lett. **86**, 4056 (2001).
[4] T. Hallam *et al.*, Phys. Rev. Lett. **103**, 256803 (2009).
[5] Y. Sato *et al.*, Phys. Rev. Lett. **97**, 106802 (2006).
[6] L. Zhang *et al.*, Phys. Rev. Lett. **101**, 155501 (2008).
[7] I. Repins *et al.*, Prog. Photovoltaics **16**, 235 (2008).
[8] U. Rau, K. Taretto, and S. Siebentritt, Appl. Phys. A **96**, 221 (2009).
[9] J. Y. W. Seto, J. Appl. Phys. **46**, 5247 (1975).
[10] S. Siebentritt and S. Schuler, J. Phys. Chem. Solids **64**, 1621 (2003).
[11] L. K. Fionova and A. V. Artemmyev, *Grain Boundaries in Metals and Semiconductors* (Les Editions Physique, France, 1993).
[12] By the subscript ''tet'' we denote directions and planes in the tetragonal system and by ''cub'' in the cubic system.
[13] C. Persson and A. Zunger, Phys. Rev. Lett. **91**, 266401 (2003).
[14] C. Persson and A. Zunger, Appl. Phys. Lett. **87**, 211904 (2005).
[15] J. E. Jaffe and A. Zunger, Phys. Rev. B **64**, 241304(R) (2001).
[16] S. B. Zhang and S.-H. Wei, Phys. Rev. B **65**, 081402(R) (2002).
[17] Y. Yan, R. Noufi, and M. M. Al-Jassim, Phys. Rev. Lett. **96**, 205501 (2006).
[18] Y. Yan *et al.*, Phys. Rev. Lett. **99**, 235504 (2007).
[19] S. Siebentritt *et al.*, Phys. Rev. Lett. **97**, 146601 (2006).
[20] K. Taretto and U. Rau, J. Appl. Phys. **103**, 094523 (2008).
[21] M. Gloeckler, J. R. Sites, and W. K. Metzger, J. Appl. Phys. **98**, 113704 (2005).
[22] M. Hafemeister *et al.*, Mater. Res. Soc. Symp. Proc. **1012**, Y09-04 (2007).
[23] T. R. Albrecht, P. Grütter, D. Horne, and D. Rugar, J. Appl. Phys. **69**, 668 (1991).
[24] Ch. Sommerhalter *et al.*, Appl. Phys. Lett. **75**, 286 (1999).
[25] N. N. Syrbu, M. Bogdanash, V. E. Tezlevan, and I. Mushcutariu, Physica (Amsterdam) **229B**, 199 (1997).
[26] L. Mandel, R. D. Tomlinson, M. J. Hampshire, and H. Neumann, Solid State Commun. **32**, 201 (1979).
[27] N.C.-C. Lu, L. Gerzberg, C.-Y. Lu, and J. D. Meindl, IEEE Trans. Electron Devices **30**, 137 (1983).
[28] M. K. Sharma and D. P. Joshi, J. Appl. Phys. **102**, 033704 (2007).
[29] To obtain a value for the barrier height, the barrier width has to be fixed for the transport modeling. We decided to use 3 lattice planes, as this corresponds to the stacking sequence of *ABCABC*. The distance of the $\{111\}_{tet}$ planes is 2.56 Å and that of the $\{112\}_{tet}$ planes is 3.21 Å.
[30] J. H. Davis, *The Physics of Low-dimensional Semiconductors* (Cambridge University Press, Cambridge, U.K., 1998).
[31] M. Morkel *et al.*, Appl. Phys. Lett. **79**, 4482 (2001).
[32] M. Bär *et al.*, Appl. Phys. Lett. **93**, 244103 (2008).
[33] S. Sadewasser *et al.*, Thin Solid Films **431–432**, 257 (2003).
[34] D. Fuertes Marrón *et al.*, Phys. Rev. B **71**, 033306 (2005).
[35] C.-S. Jiang *et al.*, Appl. Phys. Lett. **84**, 3477 (2004).
[36] D. Abou-Ras, S. Schorr, and H. W. Schock, J. Appl. Crystallogr. **40**, 841 (2007).